Nucleation and growth: Decay of a metastable state

Celeste Sagui, Dean Stinson O'Gorman, and Martin Grant

Centre for the Physics of Materials, Physics Department, Rutherford Building, McGill University, 3600 rue University, Montréal, Québec, Canada H3A 2T8

(Received 11 December 1996)

We present a self-consistent model that describes the entire process of phase separation from the initial nucleation to the late stage Ostwald ripening regime. The model, formulated in terms of a set of interface equations, naturally incorporates the correlations which originate in the overlapping of the diffusional fields corresponding to the different precipitates. [S1063-651X(97)51907-6]

PACS number(s): 64.60.My, 64.75.+g

A metastable state evolves towards its stable equilibrium state via the formation and growth of droplets. At present, the early-time process of homogeneous nucleation is well understood [1–4]. The critical energy for the formation of a droplet is determined through a competition between a volume term (which favors creation of the droplet), and a surface term (which favors its dissolution): Droplets of size $R>R_c$ (critical radius) grow, while droplets with $R<R_c$ shrink. Ostwald ripening, the late-stage process of droplet growth by evaporation and condensation, is also well understood. To reduce the interfacial free energy of the system, material diffuses away from small, high-curvature droplets (which dissolve), and condenses onto large, low-curvature droplets (which grow). The classic theory of this process is due to Lifshitz and Slyozov [5], who considered the noninteracting limit with volume fraction $\phi\to 0$. For nonzero ϕ, the main results [6,7] are that the universal scaling form of the droplet distribution function depends on ϕ, and that the coarsening rate $K(\phi)$ in the growth law for the mean radius $\overline{R(t)}$, $\overline{R^3}(t)\propto K(\phi)t$, is a monotonically increasing function of ϕ.

Although these limiting cases are understood, much less is known about the complete evolution of the system from the early nucleation to the late Ostwald ripening stage. This problem was first studied in the seminal work of Langer and Schwartz [8], who used a mean-field approach to study the nonlinear dynamical equations of a phase separating system with both nucleation and growth of droplets [9]. Experimental evidence [10] points to the importance of the interparticle diffusional interactions and of the spatial locations of particles on nucleation and growth, and therefore, to the need for a comprehensive theory including such correlation effects.

In this paper, we present a self-consistent model that combines steady-state homogeneous nucleation theory with the classical Lifshitz-Slyozov mechanism, modified to account for the substantial correlations amongst the droplets. The model, formulated in terms of a set of interface equations, is numerically studied in dimensions $d=2$ and $d=3$. Since our method only integrates the interface equations, it permits the simulation of much larger systems than can be studied using other methods, such as Langevin equation simulations. Our formalism naturally incorporates the crossover from the early-stage nucleation to the late-stage scaling regime, without *ad hoc* assumptions. Results from a mean-field solution based on a Thomas-Fermi approximation are also shown.

We use dimensionless variables. Units of length and time are expressed in terms of the capillary length $l_c=(d-1)\sigma v_m/(kT)$ and the characteristic time $t_c=l_c^2/[DC_{eq}(\infty)v_m]$. These quantities depend on the spacial dimension d, the surface tension σ, the molecular volume v_m, the temperature T, the Boltzmann constant k, the solute concentration in the matrix at a planar interface $C_{eq}(\infty)$ of a phase-separated system, and the diffusion constant D. We also introduce a dimensionless concentration field $\theta(\mathbf{r},t)=[C(\mathbf{r},t)-C_{eq}(\infty)]/C_{eq}(\infty)$, whose value far from any droplet is the time-dependent supersaturation $\chi(t)$; and the dimensionless parameter [8] $\chi_0^{d-1}=v\sigma l_c^{d-1}/(kT)$ where $v=\pi^{d/2}/\Gamma(d/2+1)$. In dimensionless form, the field-theoretic steady-state nucleation rate can be written as [2,8,11]

$$J_d=A_d[\chi(t)/\chi_0]^{\alpha_d}\beta_d\exp\{-[\chi_0/\chi(t)]^{d-1}\} \qquad (1)$$

where A_d is a numerical constant, $\alpha_3=2/3$, $\alpha_2=4$, $\beta_3=[1+\chi(t)/\chi_0]^{3.55}$, and $\beta_2=1$. The critical radius is given by $R_c=1/\chi(t)$. The nucleation rate gives the number of droplets nucleated per unit volume per unit time for a given supersaturation.

The time evolution of the system is described by the multidroplet diffusion equation for the concentration field $\theta(\mathbf{r},t)$. In the monopole approximation,

$$\frac{\partial\theta(\mathbf{r},t)}{\partial t}-\nabla^2\theta(\mathbf{r},t)=-a\sum_{i=1}^{N(t)}Q_i\delta(\mathbf{r}-\mathbf{r}_i), \qquad (2)$$

where $a=vd$ and the coefficients Q_i describe the strength of the source or sink of the current for diffusion. We assume spherical droplets in local equilibrium, so that the concentration at the interface is determined by the Gibbs-Thompson boundary condition $\theta(\mathbf{R}_i)=1/R_i$. The late-time, quasistatic solution of Eq. (2) is given by the sum of the source terms (i.e., the ''charges'' Q_i multiplied by the appropriate Green's function) plus the supersaturation $\chi(t)$, which is slaved to the inverse mean radius: $\overline{R(t)}\simeq R_c=1/\chi(t)$ [7]. We can write an approximate solution to Eq. (2) by introducing a coefficient $Q_0(t)$, which tracks the evolution of $\chi(t)$. [At

late times, $Q_0(t)=\chi(t)$]. In $d=3$, this solution is evaluated on the surface of droplet i, giving

$$\frac{1}{R_i}=Q_0(t)-\frac{Q_i}{R_i}-\sum_{j\neq i}\frac{Q_j}{|\mathbf{r}_i-\mathbf{r}_j|}, \tag{3}$$

where $\mathbf{r}_j$ is the center of mass of droplet j. The radial growth law comes from a local continuity equation in a volume enclosing only one droplet:

$$R_i^{d-1}(dR_i/dt)=Q_i. \tag{4}$$

Since the conservation of mass requires that $\chi(t)+v\Sigma_{i=1}^{N(t)}R_i^d=\phi$, where ϕ is the constant volume fraction of the minority phase, the variation of supersaturation is

$$\frac{\partial\chi(t)}{\partial t}+a\sum_{i=1}^{N(t)}Q_i+\left.\frac{\partial\chi(t)}{\partial t}\right|_{nuc}=0. \tag{5}$$

The third term is the decrease of $\chi(t)$ due to nucleation of droplets. The second term accounts for the variation of $\chi(t)$ due to growth or dissolution of existing droplets. This diffusive variation of $\chi(t)$ is treated in a mean-field approximation which gives $\Sigma_i Q_i=N[\overline{R}(t)\chi(t)-1]$ in $d=3$. Equations (3) and (5) comprise a set of $N+1$ linear coupled equations for the coefficients Q_i and Q_0. Together with the growth equation (4) and the nucleation rate equation (1), they constitute a formal solution to the nucleation and growth problem, which should well describe the solid-state precipitation of a binary alloy. The numerical solution of similar sets of self-consistent equations has been described previously [7,12]. For the particular case of homogeneous nucleation, the time evolution starts in an initial supersaturated state, $\chi(0)=\phi$. The equations are integrated numerically using an Euler discretization scheme with a variable time increment dt. At a given instant t, the nucleation rate $J_d[\chi(t)]$, the critical radius $R_c(t)$, and the growth law (4), are used to compute the minimum time required to nucleate or eliminate one droplet. This in turn determines $\partial\chi/\partial t|_{nuc}$. Radii R_i and supersaturation $\chi(t)$ are updated following the path of minimum dt. This updating of R_i and $\chi(t)$ modifies the minimum dt, which must be computed self-consistently. Further details are given elsewhere [13].

The time evolution is determined by three parameters: the nucleation parameter χ_0 [14], the width dR_c of the distribution function of the nucleation rate [15], and the volume fraction ϕ. The first two parameters determine the initial droplet distribution function and the subsequent crossover behavior, while the effects of ϕ persist to late times. The time evolution is divided into three stages: a nucleation, a diffusive growth and a coarsening stage. Nucleation of droplets produces the initial depletion of the supersaturation. While nucleation is proceeding, the first nuclei start to grow, seizing material from the background supersaturation. The diffusive growth stage is marked by the high increase or decrease in slope of $\overline{R}(t)$ or $\chi(t)$, and by a nearly constant droplet density $n(t)$. When the supersaturation is sufficiently reduced, its role is confined to mediating the exchange of material between the individual droplets. Growth is a global, interactive phenomenon, and time evolution proceeds via Ostwald ripening.

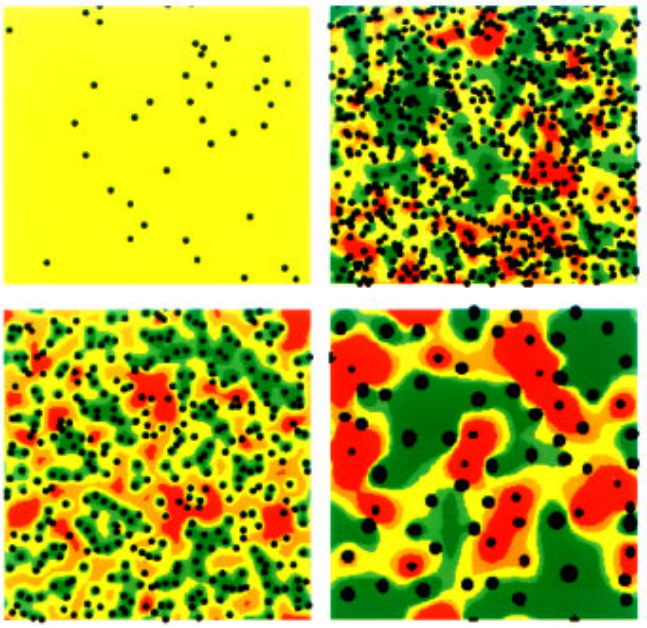

FIG. 1. (Color) Time evolution for a $d=2$ system of dimensionless edge length 20 454 with $\phi=0.05$ and $\chi_0=1/2$. Top left: nucleation regime ($t=9500$). Top right: configuration for the maximum number of droplets ($t=1.15\times10^5$). Bottom left: diffusive growth regime ($t=4.79\times10^5$). Bottom right: ripening regime ($t=5.7\times10^7$). For $a\leqslant[\theta(\mathbf{r},t)-\chi(t)]/\chi(t)<b$, the color scheme is as follows. Dark green: $b=-0.08$; light green: $a=-0.08$, $b=-0.04$; yellow: $a=-0.04$, $b=0.04$; orange: $a=0.04$, $b=0.12$; red: $a=0.12$. Large droplets are generally in the green region, where there is depletion of the supersaturation, while disintegrating droplets are in the red regions of high diffusion fields.

Figure 1 shows the droplets and background diffusion field for the time evolution of a sample $d=2$ system. In the initial nucleation regime, the background is homogeneous. When the number of droplets $N(t)$ reaches its maximum, the structure in the background signals the imminent decay of $N(t)$. In the diffusive regime, most droplets are growing (and they are located in the depleted green regions). Finally, the ripening regime shows a clearly correlated structure in the background. Figure 2 shows the dependence of the mean radius $\overline{R}(t)$, the droplet number density $n(t)$, and the supersaturation $\chi(t)$ on χ_0 and ϕ for a $d=3$ system. Similar results are obtained in $d=2$ systems. The top row compares different values of χ_0 [14], (1/7, 1/6, 1/5, and 1/4.5) with a volume fraction $\phi=0.05$, while the bottom row compares different values of ϕ (0.04, 0.065, and 0.083) at constant $\chi_0=1/6$. As expected, the nucleation parameters χ_0 and dR_c are irrelevant for the late stages, and the functions $\overline{R}(t)$, $n(t)$, and $\chi(t)$ collapse into a ϕ-dependent universal function. The crossover to the scaling form, however, can take several decades in time. The nucleation rate is $J_d\propto\exp[-E_c/(kT)]$, where $E_c/(kT)=[\chi_0/\chi(t)]^{d-1}$ is the droplet activation energy, which causes very different initial and intermediate behavior. We consider two cases. (i) *Large values* of E_c ($\geqslant 17kT$): These occur for $\chi_0\geqslant 1/4.5$ in the upper panel ($\phi=0.05$), or for $\phi\leqslant 0.04$ in the lower panel

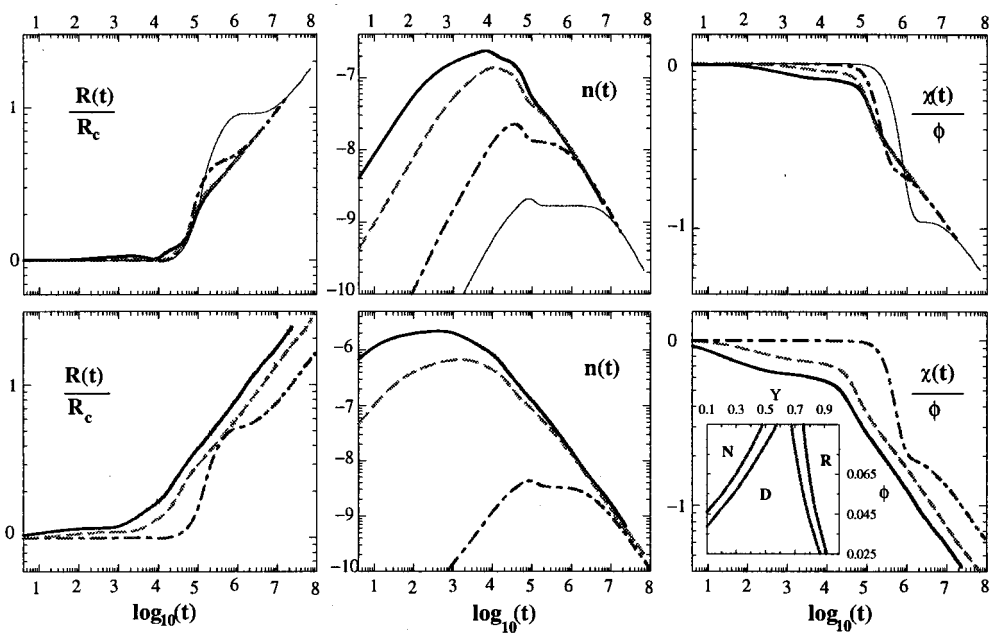

FIG. 2. Left, middle, and right panels show log-log plots for the normalized mean radius $\overline{R(t)}/R_c$, the droplet number per unit volume $n(t)$, and the normalized supersaturation $\chi(t)/\phi$ for a $d=3$ system. Here $R_c=R_c(t=0)=1/\phi$. Top row: $\phi=0.05$ and $\chi_0=1/7$ (thick solid line), 1/6 (long-dashed line), 1/5 (dotted-dashed line), and 1/4.5 (thin solid line). The nucleation rate width is chosen as $dR_c=0.05R_c$. Bottom row: $\chi_0=1/6$ and $\phi=$ 0.083 (thick solid line), 0.065 (long-dashed line) and 0.04 (dotted-dashed line); $dR_c=(\sqrt{6}\chi_0)^{-1}$. The inset shows a schematic diagram of the different regimes, nucleation (**N**), diffusion (**D**), and ripening (**R**) as function of the volume fraction ϕ and the nucleated volume $X=1-\chi(t)/\phi$. The narrow regions between **N** and **D** and between **D** and **R** indicate a crossover between the corresponding regimes.

($\chi_0=1/6$).(ii) *Low values* of E_c ($\leqslant 11kT$): These occur for $\chi_0\leqslant 1/6$ when $\phi=0.05$ or for $\phi\geqslant 0.05$ when $\chi_0=1/6$. In this latter case, the nucleation rate increases and the maximum of $n(t)$ is higher and occurs sooner with decreasing χ_0 and increasing ϕ. Instead, in the first case, nucleation is very sluggish. For instance, at $t\sim 10^5$, the value of $\chi(t)$ for $\chi_0=1/4.5$ is still very large and the few droplets nucleated have nearly equal radii. The excess of supersaturation is eliminated by the positive growth of all droplets, which hardly interact. Thus their number stays constant while $\overline{R(t)}$ and $\chi(t)$ abruptly increase and decrease respectively. During this stage, which lasts about a decade, the droplet distribution function is quite narrow. For $t>10^6$, $\chi(t)$ has decreased substantially, and droplets can no longer grow at its expense. Ostwald ripening then takes over as the dominant mechanism of phase separation. However, because the droplet distribution function is still narrow, it takes some time for the system to develop a proper dispersion of radii, large enough for $n(t)$ to decrease. During this time $\chi(t)$ and $\overline{R(t)}$ are nearly constant. When E_c is small, there is a large initial depletion of $\chi(t)$ due to nucleation. If, in addition, ϕ is small, diffusive growth is minor, favoring a relative early onset of Ostwald ripening with its characteristic power-law behavior. If ϕ is relatively large, both mechanisms of diffusive growth and ripening are present until very late times. The inset shows a schematic diagram of the different regimes, nucleation, diffusive growth and ripening, and their corresponding crossover regions, as function of ϕ and the nucleated volume $X=1-\chi(t)/\phi$.

Some initial and intermediate times for the radius distribution functions $f(R,t)$ for $\phi=0.05$ and $\chi_0=1/6$ are shown

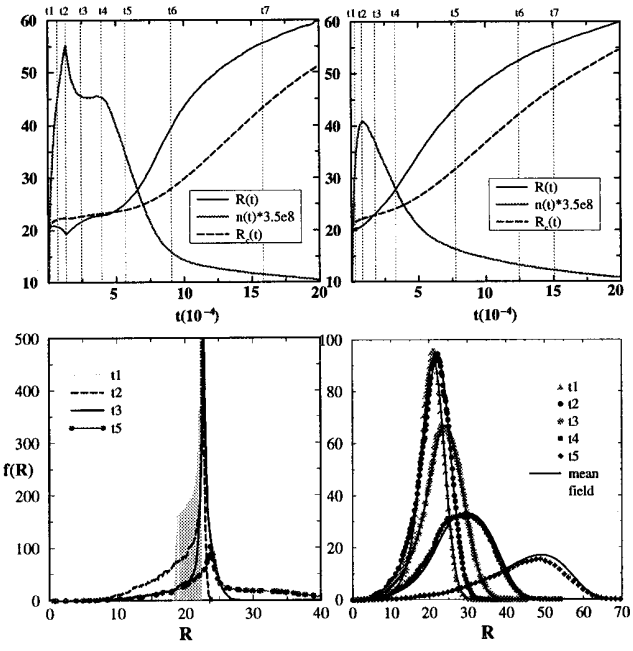

FIG. 3. For $\phi=0.05$ and $\chi_0=1/6$, top panels show $\overline{R(t)}$, the droplet number per unit volume $n(t)$, and the critical radius $R_c(t)=1/\chi(t)$. The vertical bars indicate the time at which the droplet distribution functions are depicted in the lower panels. Left column: $dR_c=0$. Right column: $dR_c=(\sqrt{6}\chi_0)^{-1}$. The solid line represents the results of a mean-field theory that we developed to include the droplet correlation effects.

in Fig. 3. The top panels show $\overline{R(t)}$, $n(t)$, and the critical radius $R_c(t)=1/\chi(t)$. The vertical bars indicate the time at which the droplet distribution functions are depicted in the lower panels. The left- and right-hand columns show the role of the width of the nucleation rate dR_c for the early times. The left-hand column corresponds to $dR_c=0$, i.e., when all the droplets are nucleated with the critical radius. This extreme situation depicts clearly the different mechanisms of nucleation, growth and ripening. With the nucleation of critical droplets, $f(R,t)$ develops a high peak centered at R_c. As supersaturation diminishes, R_c increases and the newly nucleated droplets have larger radii than the older ones, so that $f(R,t)$ is asymmetric, as shown in $f(R,t=t1)$. Before the peak of $n(t)$ at $t2$, none of the nucleated droplets has disappeared, and $f(R,t=t2)$ has a high peak for $R>\overline{R(t)}$ and a long tail for $R<\overline{R(t)}$. This excessive population of small droplets causes $\overline{R(t)}$ to decrease towards the kink at $t2$. Immediately after $t2$, these small droplets dissolve, $n(t)$ decreases and $\overline{R(t)}$ increases sharply while $f(R,t)$ is almost symmetric with a small tail for $R<\overline{R(t)}$. The dissolution of the small droplets allows a $\chi(t)$ high enough to nucleate new droplets. Intensive nucleation and dissolution of small droplets occurs between $t2$ and $t4$ and the new droplets produce the second kink of $n(t)$ at $t4$. The coarsening of droplets produces a hump in $f(R,t)$ for $R>\overline{R(t)}$, which becomes a second peak between $t4$ and $t5$, creating a bimodal distribution and a second kink in $\overline{R(t)}$. At exactly this point, $R_c(t)$ crosses $\overline{R(t)}$, ending a subcritical stage, with many droplets smaller than the critical size. After $t5$ the peak for $R<\overline{R(t)}$ rapidly decreases, while the coarsening peak increases and moves towards larger R's. The right-hand column in Fig. 3 shows the case with $dR_c=(\sqrt{6}\chi_0)^{-1}$. The mechanisms are similar but ''washed out'' due to the dispersion in radii, and the subcritical stage ends sooner. The solid line distribution functions represent our mean-field solution to the equations, based on a Thomas-Fermi approximation [13].

In summary, we have introduced a self-consistent model that describes the entire process of phase separation from the initial nucleation regime to the late stage Ostwald ripening regime. The model naturally incorporates the correlations which originate in the overlapping of the diffusional fields of each precipitate. A good experimental candidate to test our results would be a lattice-matched binary alloy during solid-state precipitation.

This work was supported by the Natural Sciences and Engineering Research Council of Canada, and le Fonds pour la Formation de Chercheurs et l'Aide à la Recherche du Québec.

[1] M. Volmer and A. Weber, A. Phys. Chem. **119**, 277 (1926); L. Farkas, Z Phys. Chem. (Munich) **125**, 236 (1927); R. Becker and W. Döring, Ann. Phys. (N.Y.) **24**, 719 (1935); R. Kaischew and I.N. Stranski, Z. Phys. Chem. **26**, 81 (1935); J.B. Zeldovich, Acta Physicochim. URSS **18**, 1 (1943).

[2] J.S. Langer, Ann. Phys. (N.Y.) **41**, 108 (1967); *ibid.* **54**, 258 (1969); S. Coleman, Phys. Rev. D **15**, 2929 (1977).

[3] N.C. Wong and C.M. Knobler, J. Chem. Phys. **69**, 725 (1978); E.D. Siebert and C.M. Knobler, Phys. Rev. Lett. **52**, 1133 (1984); *ibid.* **54**, 819 (1985).

[4] D.W. Herrmann, *et al.* Phys. Rev. Lett. **49**, 1262 (1982); D. Stauffer, A. Coniglio, and D.W. Herrmann, *ibid.* **49**, 1299 (1982).

[5] I.M. Lifshitz and V.V. Slyozov, J. Phys. Chem. Solids **19**, 35 (1961).

[6] J.A. Marqusee and J. Ross, J. Chem. Phys. **80**, 536 (1984); P.W. Voorhees, J. Stat. Phys. **38**, 231 (1985); C.W.J. Beenaker, Phys. Rev. A **33**, 4482 (1986); Y. Enomoto, *et al.* Acta. Metall. **34**, 2119 (1986); M. Marder, Phys. Rev. A **36**, 858 (1987); A.J. Ardell, Phys. Rev. B **41**, 2554 (1990); N. Akaiwa and P.W. Voorhees, Phys. Rev. E **49**, 3860 (1994).

[7] J.H. Yao, *et al.* Phys. Rev. B **45**, 8173 (1992).

[8] J.S. Langer and A.J. Schwartz, Phys. Rev. A **21**, 948 (1980).

[9] More recently, Tokuyama and Enomoto [M. Tokuyama and Y. Enomoto, Phys. Rev. Lett. **69**, 312 (1992)] studied the evolution of a $d=3$ system after heterogeneous nucleation. They considered the effects of correlations through a perturbative expansion in ϕ.

[10] P.W. Voorhees and R.J. Schaefer, Acta Metall. **35**, 327 (1987).

[11] N.J. Günther *et al.*, J. Phys. A **13**, 1755 (1980).

[12] C. Sagui and R.C. Desai, Phys. Rev. Lett. **74**, 1119 (1995).

[13] C. Sagui *et al.* (unpublished).

[14] The relation between χ_0 and that used by Langer and Schwartz, χ_0^*, is $\chi_0=(\beta/2)\chi_0^*$, where β is the critical exponent for temperature dependence of the concentration near the critical temperature ($\Delta C\sim|T-T_c|^{\beta}$). Since $\beta=1/3$ and $\chi_0^*\sim 1$ then $\chi_0\sim 1/6$ in $d=3$.

[15] To compare with the standard literature, we choose the droplet radius from a Gaussian distribution centered at R_c, with a width dR_c. This width is usually determined by assuming an uncertainty in the activation energy of the order of kT, which gives a width $dR_c=(\sqrt{6}\chi_0)^{-1}$ in our units. A further discussion is given in Ref. 13.